Predicting the Thermal Conductivity of AlSi/Polyester Abradable Coatings: Effects of the Numerical Method

Rodolphe Bolot, Jean-Louis Seichepine, Jiang Hao Qiao, and Christian Coddet

The final target of this study is to achieve a better understanding of the behavior of thermally sprayed abradable seals such as AlSi/polyester composites. These coatings are used as seals between the static and the rotating parts in aero-engines. The machinability of the composite coatings during the friction of the blades depends on their mechanical and thermal effective properties. In order to predict these properties from micrographs, numerical studies were performed with different software packages such as OOF developed by NIST and TS2C developed at the UTBM. In 2008, differences were reported concerning predictions of effective thermal conductivities obtained with the two codes. In this article, a particular attention was paid to the mathematical formulation of the problem. In particular, results obtained with a finite difference method using a cell-centered approach or a nodal formulation allow explaining the discrepancies previously noticed. A comparison of the predictions of the computed effective thermal conductivities is thus proposed. This study is part of the NEWAC project, funded by the European Commission within the 6th RTD Framework programm (FP6).

1. Introduction

Thermal spray technologies allow elaborating coatings on surfaces for protection against corrosion, wear, or high temperature environments. Thermal spray processes consist in spraying molten drops of the protective material on the substrate surface. The produced coatings consist of a network of intermingled splats formed by the flattening and solidification of the molten droplets. They present a complex architecture comprising thin inter-lamellar cracks, globular pores, and intra-lamellar cracks (for ceramics) generated by thermal stresses. Moreover, depending on the process and nature of the sprayed material, they may also contain partially molten particles,

as well as oxides (for metals and alloys). From that complex architecture, thermal spray coatings exhibit effective properties strongly different from those of the bulk material from which they are made of. Subsequently, estimation of these effective properties (thermal and mechanical) presents a huge interest. For the particular case of the thermal properties, experimental techniques such as the flash method (Ref 1-3) are often applied to estimate the thermal diffusivity from which the effective conductivity may then be deduced. Moreover, many heuristic correlations have also been suggested in the literature to estimate the effective thermal conductivity of porous materials. These correlations relate the effective thermal conductivity to the pore content (Ref 4-12). In the case of spherical pores, correlations of the type $\kappa/\kappa_0 = 1 - \alpha p$ or $\kappa/\kappa_0 = (1 - p)^\beta$ have been suggested (Ref 4-8), in which κ is the effective thermal conductivity of the porous material, κ_0 is the thermal conductivity of the bulk material, p represents the pore level, and α and β are dimensionless coefficients.

In the case of thermal spray coatings, pores may also be considered as ellipsoids (Ref 10-12). McPherson (Ref 13) correlated the loss of conductivity of plasma sprayed ceramic coatings versus the limited contact area between the lamellae: the noncontact regions represent thin planar pores presenting a low thermal conductivity in comparison with that of the solid matrix. Boire-Lavigne et al. (Ref 14) adapted the contact area approach of McPherson to the case of tungsten coatings and noticed a strong influence of the spraying atmosphere. For the case of ceramic coatings again, the works of Sevostianov et al. (Ref 15-20) allow to estimate the effective properties versus a few structural parameters of the microstructure among which the pore orientation is for example taken into account. Still for

Rodolphe Bolot, Jean-Louis Seichepine, Jiang Hao Qiao, and **Christian Coddet**, LERMPS, University of Technology of Belfort-Montbéliard, Belfort, Montbéliard, France. Contact e-mail: rodolphe.bolot@utbm.fr.

ceramics, the works of Golosnoy et al. (Ref 21, 22) consider the parameter of contact between the lamellae by the notion of bridges through the thin inter-lamellar pores also introduced by Litovsky et al. (Ref 23-26).

Nevertheless, most of the mentioned works concern ceramics for which the loss in the effective thermal conductivity depends strongly on the thin inter-lamellar cracks between lamellae in the case of thermal spray coating. In the case of abradable materials such as AlSi/polyester coatings, the decrease in the effective thermal conductivity is mainly provided by the presence of the polyester phase which presents a much lower conductivity than the AlSi alloy. In parallel to these theoretical and experimental investigations, characterization techniques based on numerical methods have been developed successfully: in this case, images of the coating cross-sections are used as mesh-support to perform calculation using either finite element (Ref 27-33) or finite difference (Ref 34-39) methods.

In this context, it is obvious that estimation of the effective properties of thermally sprayed coatings presents a large interest and particularly in the aeronautic industry for which the behavior of abradable coatings used as seals between the static and rotating parts of the aircraft engines must be integrated. Global air traffic is forecast to grow at an average annual rate of around 5% in the next 20 years. This high level of growth makes the need to address the environmental penalties of air traffic all the more urgent. As a result, Europe's aviation industry faces a massive challenge to satisfy this demand for increased air travel in an economic and safe way. Therefore, alternative engine configurations need to be researched to find a significant and permanent reduction of pollution. NEWAC (Ref 40) is a European-level programme, under the leadership of MTU Aero Engines, in which major European engine manufacturers, assisted by universities, research institutes, and enterprises (40 partners in all) have focussed on new core engine concepts. The project was funded by the European Commission within the 6th RTD Framework Programm (FP6). The main NEWAC result is to validate novel technologies enabling a 6% reduction in CO_2 emissions and a further 16% reduction in NO_X emissions.

The role of UTBM within this programme concerns a part of the 5th work package (subsection modelling the abradable and its wearing). In particular, we contributed to a better estimation of effective properties of AlSi/polyester abradable seals. In order to do so, some calculations were performed on the basis of micrographs of coatings using both OOF2 and TS2C. Object-Oriented Finite Element Analysis of Microstructures (OOF) is a software package developed by National Institute of Standards and Technology (NIST) and commonly used in this field of applications (Ref 29-33), whereas TS2C is an in-house code developed at the UTBM whose actual capabilities focus on estimation of the thermal conductivity of thermally sprayed coatings (Ref 35-39). A poster was presented during EUROMAT (Nurnberg, Germany, September 2007) on this subject: this poster is available on the website of the NEWAC programme (Ref 41). In 2008,

a first article dealing with estimation of the thermal conductivity of AlSI/polyester abradable seals was presented (Ref 42). This article was awarded during the conference and a completed version was also published in 2009 (Ref 44). However, some discrepancies were noticed concerning the results predicted using OOF2 and TS2C: these differences were not explained up to now so that one of the objectives of this study is to provide explanations concerning this point, to inform the users of the numerical tools specialized in this domain.

2. Summary of the Previous Results

Some pictures of coating cross sections taken at different magnification levels were considered to perform numerical estimations of the effective thermal conductivity of AlSi/polyester abradable coatings (Ref 42, 44). The coatings were produced with two different powders (i.e., Durabrade 1605 and Metco 601 NS) whose composition is a blend of AlSi alloy (12 wt.% of Si) and polyester (40 wt.% in the powder). Three different magnification levels were first considered. According to the results, the covered area was not sufficient for the two largest magnification levels. Subsequently, the more the covered area is low, the highest the predicted thermal conductivity is, because of the increase in the continuity of the AlSi phase. On the contrary, for the lowest resolution level (magnification of 50 corresponding to a resolution of 3 μm/pixel), the covered area becomes sufficient to obtain a good representation of the discontinuity of the AlSi phase, thus providing more accurate results concerning the predicted thermal conductivity. For the present application, the minimum representative length scale was thus of about 2 mm in the transverse direction. Below this value, the considered volume is not representative of the material.

In all results reported in this previous article, a Despeckle filtering was applied to the original binary images produced from the microstructures until a stable image was reached. This step was initially done to simplify the design of the porous network to attempt describing it on the basis of ellipsoids. The thermal conductivity of AlSI12 phase was assumed to be of $130 \text{ W} \cdot \text{m}^{-1} \cdot \text{K}^{-1}$. This value is medium between the thermal conductivity of Die Casting AlSi12 (i.e., $122 \text{ W} \cdot \text{m}^{-1} \cdot \text{K}^{-1}$) (Ref 45, 46) and the one of alloy Al4032 (i.e., $138 \text{ W} \cdot \text{m}^{-1} \cdot \text{K}^{-1}$) (Ref 45). Concerning the polyester phase, a value of $0.17 \text{ W} \cdot \text{m}^{-1} \cdot \text{K}^{-1}$ (Ref 44, 46) was applied.

Because of the high consumption of RAM, the computations performed with OOF2 could not be obtained for the original resolution of the different images: the use of a computer equipped with 2 Go of RAM did not allow considering pictures exceeding 250,000 pixels when using a 1 cell/pixel formulation of the problem (OOF also allows defining meshes formed by triangles or quadrangles grouping several pixels). For this reason, the results produced with the two codes were compared for intermediate resolutions only. At present, the use of a recent computer

equipped with 4 Go of RAM allowed treating most of the pictures presented in this previous article: the reason being that the limiting value of the number of pixels is now around 410,000 cells, which corresponds to the largest images considered in the article. In all cases, the limiting value is not sensitive versus the LINUX distribution: Ubuntu, Mint, OpenSuse, or Fedora can be used indifferently to install and run OOF2. Nevertheless, for applications for which the RAM may represent a problem, the use of a 32 bit distribution of Linux is advised because the RAM is burned much faster with 64 bit distributions.

Table 1 presents a synthesis of the results obtained with the two codes for the picture showed in Fig. 1. The original resolution of the picture is 756×541 pixels. The values were obtained assuming a thermal conductivity of $130 \; W \cdot m^{-1} \cdot K^{-1}$ for the AlSi phase and of $0.17 \cdot W \cdot m^{-1} \cdot K^{-1}$ for the polyester phase.

Despite the differences, the most interesting point is that the difference between the values computed with the two codes represents about 30% at the lowest resolution of 25%, 11% at the resolution of 50%, 7% at the resolution of 75%, and becomes lower that 4% at the maximum resolution (0.467 for TS2C against 0.485 for OOF2). Thus, one may easily observe a convergence tendency which is very comforting.

3. Cell-Centered and Nodal Discretization Methods Within TS2C

All computations performed up to 2008 with TS2C (Ref 35-38) were obtained using a cell-centered formulation of the problem. In this study, a different methods based on a nodal formulation was specially developed for comparison. The reason for these new developments is that FE-based codes such as OOF2, implement a nodal formulation of the problem in contrast with finite difference-based models. In practice, it was found to be the reason explaining the differences between the results obtained with the two codes.

Under stationary conditions, the 2D heat conduction problem through a heterogeneous material can be expressed as

$$-\frac{\partial}{\partial x}\left(\kappa \frac{\partial T}{\partial x}\right) - \frac{\partial}{\partial y}\left(\kappa \frac{\partial T}{\partial y}\right) = 0$$

Figure 2 presents a schematic view of the discretization over one cell (pixel for the present application) for cell-centered and nodal formulations, respectively.

Because the pixels are in series, the thermal resistances are additive and the cell-centered formulation results in a linear equation derived for each pixel as follows:

$$Ap(i,j)T(i,j) = Ax(i,j)T(i-1,j)$$
$$+ Ax(i+1,j)T(i+1,j)$$
$$+ Ay(i,j)T(i,j-1) + Ay(i,j+1)T(i,j+1)$$

with

$$Ax(i,j) = \frac{2}{\frac{1}{\kappa(i,j)} + \frac{1}{\kappa(i-1,j)}}$$

and

$$Ay(i,j) = \frac{2}{\frac{1}{\kappa(i,j)} + \frac{1}{\kappa(i,j-1)}}$$

and

$$Ap(i,j) = Ax(i,j) + Ax(i+1,j) + Ay(i,j) + Ay(i,j+1)$$

A system is formed by writing a similar equation for each pixel and the boundary conditions are taken into account by acting over some equations such as those corresponding to the pixels pertaining to the top and bottom lines of the image (for example).

In contrast, the temperatures are calculated at the corners of the cells (i.e., of the pixels) for the nodal formulation so that the pixels are in parallel.

Thus, for the nodal formulation the Ax and Ay coefficients may now be calculated as:

$$Ax(i,j) = \frac{\kappa(i,j) + \kappa(i,j+1)}{2}$$

and

$$Ay(i,j) = \frac{\kappa(i,j) + \kappa(i+1,j)}{2}$$

and

$$Ap(i,j) = Ax(i,j) + Ax(i+1,j) + Ay(i,j) + Ay(i,j+1)$$

In both the cases, the problem consists in solving a system of linear equations (one equation per pixel). It can be solved by applying iterative algorithms such as the SOR or LSOR procedures (Ref 35, 36) until the residuals are becoming sufficiently small.

4. Numerical Results

By applying the nodal formulation to the case considered in the previous section, the predicted thermal conductivity is $0.493 \; W \cdot m^{-1} \cdot K^{-1}$ instead of $0.467 \; W \cdot m^{-1} \cdot K^{-1}$ for the initial (i.e., cell-centered) formulation of TS2C and $0.485 \; W \cdot m^{-1} \cdot K^{-1}$ for OOF2 (see Table 1). One may say that the nodal formulation makes more than compensate the initial differences between the two codes.

Table 1 Synthesis of the results previously calculated with OOF2 and TS2C for the picture of Fig. 1 (i.e., magnification level of 50)

Resolution, %	κ_e, $W \cdot m^{-1} \cdot K^{-1}$	
	TS2C	OOF2
100	0.467	0.485 (a)
75	0.468	0.500 (b)
50	0.458	0.511
25	0.402	0.549

(a) Data never provided elsewhere
(b) Data provided in (44) but not in (42)

4.1 Influence of Despeckle Filtering and of the Discretization Method (Nodal or Cell-Centered)

The coming results were computed to analyze the effects of the mathematical formulation (i.e., nodal or cell-centered formulations), of the application of Despeckle filtering (noise reduction) and also to evaluate the sensitivity of the results versus the considered thermal conductivity of the AlSi phase.

Figure 3 presents the original microstructure, the binary picture obtained after the threshold operation and the binary picture obtained after applying Despeckle filtering for the coating produced with the Durabrade 1605 powder. One may notice that the last image (Fig. 3c) is weakly different from that shown in Fig. 1, the reason being that a slightly different threshold was applied for these recent computations (level 142/255). In practice, the binary picture produced after applying the threshold (Fig. 3b) presents a rate of polyester of 66.8% (i.e., 33.2% of AlSi).
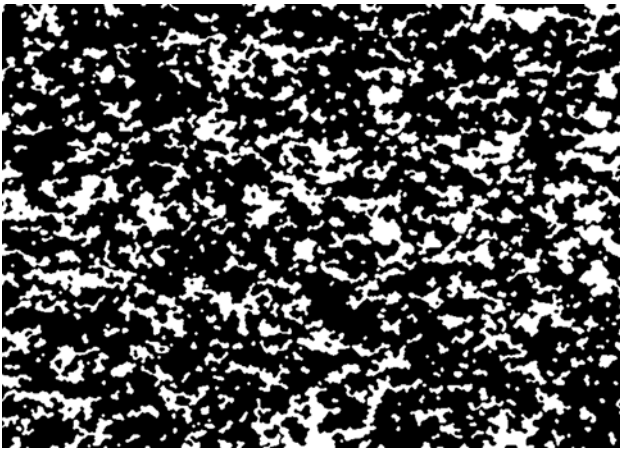
Despeckle filtering gives rise to a slight increase in the polyester content (i.e., 69.9% of polyester for the image of Fig. 3c). This value of 69.9% may also be compared to that of Fig. 1 (71.1%). Consequently, the newly generated image presents a slightly higher content of AlSi in comparison with the previously generated figure. By comparing Fig. 3(b) and (c), one may see that the small details disappeared after application of Despeckle filtering and the phase distribution looks more globular after this step.

Table 2 presents the results obtained for images of Fig. 3(b) and (c), for the cell-centered and nodal formulations implemented in TS2C and for three different values assumed for the AlSi phase (ranging from 120 to $145 \text{ W} \cdot \text{m}^{-1} \cdot \text{K}^{-1}$).

One may notice that the considered thermal conductivity of AlSi influences only slightly the resulting effective thermal conductivity of the coating (less than 1% difference between the values computed using 120 and $145 \text{ W} \cdot \text{m}^{-1} \cdot \text{K}^{-1}$). Thus, the thermal conductivity assumed for the AlSi phase does not seem to be a critical parameter.

The difference in the thermal conductivity predicted with the cell-centered and nodal formulations is larger if Despeckle filtering is not applied (about 16% difference for the raw image, against 6% for the image treated with the Despeckle filter).

The calculated effective thermal conductivities are higher for the raw image in comparison with those computed for the image treated using Despeckle filtering. By considering an average value between the cell-centered and nodal formulations of the code, one obtains $0.67 \text{ W} \cdot \text{m}^{-1} \cdot \text{K}^{-1}$ for the raw image (no Despeckle) and $0.52 \text{ W} \cdot \text{m}^{-1} \cdot \text{K}^{-1}$ for the image treated using Despeckle filtering.

Since the measured effective thermal conductivity is $0.53 \text{ W} \cdot \text{m}^{-1} \cdot \text{K}^{-1}$ for these coatings, one could simply conclude that applying Despeckle filtering is preferable. However, it is not so simple and we think that calculations performed using the raw image (Fig. 3b) are more suitable, the differences between the numerical value of

Fig. 1 View of the material distribution (white AlSi, black polyester) in the coating after applying successive Despeckle filtering operations (until convergence toward a stable picture)
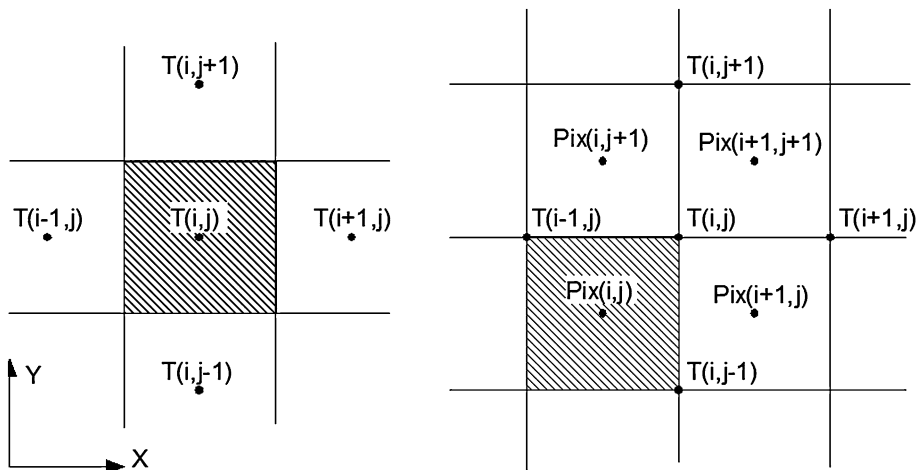

Fig. 2 Representation of the cell-centered (left) and nodal (right) discretization methods with cell indices
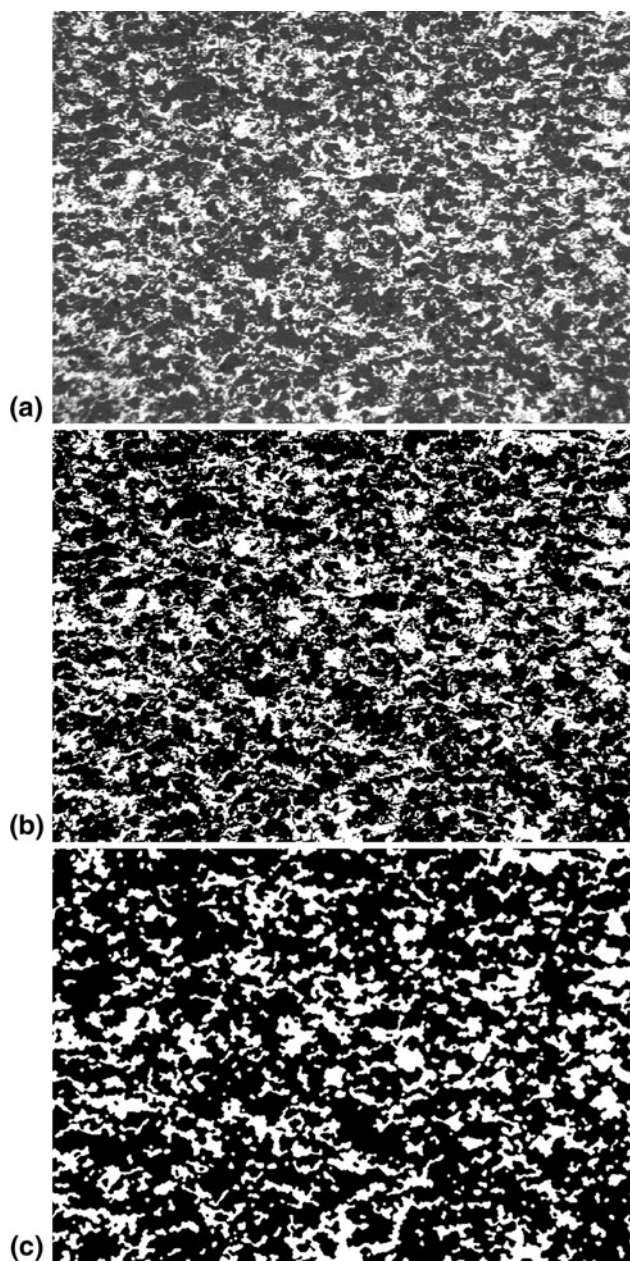
Fig. 3 Initial micrographs (a), binary picture after application of the threshold (b), and binary picture after successive applications of Despeckle filtering (c)

$0.67 \ W \cdot m^{-1} \cdot K^{-1}$ and the experimental one of $0.53 \ W \cdot m^{-1} \cdot K^{-1}$ being explained by the thermal conductivity assumed for the polyester phase. In practice, the value of $0.17 \ W \cdot m^{-1} \cdot K^{-1}$ used for the polyester phase is certainly overestimated, the reason being that this phase includes a certain level of porosity.

4.2 Case of Ternary Pictures

It was observed on the original micrographs that some groups of pixels were darker in comparison with the rest of the gray matrix. It was thus decided to try discriminating the globular pores from the polyester phase. In order to

Table 2 Predicted thermal conductivities calculated for different values of the thermal conductivity of the AlSi phase, using the cell-centered formulation of TS2C or the nodal formulation (TS2C_NF) for the binary pictures obtained after applying the threshold only or after applying successive Despeckle filtering

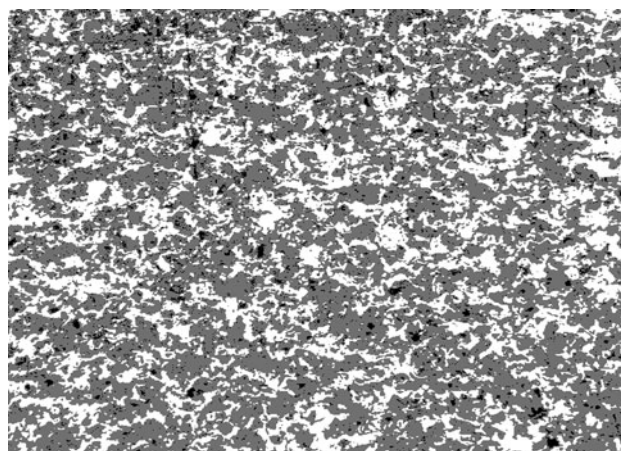| $\kappa_{polyester} = 0.17 \ W \cdot m^{-1} \cdot K^{-1}$	$\kappa_e, W \cdot m^{-1} \cdot K^{-1}$			
	Raw image—no Despeckle		After Despeckle	
$\kappa_{AlSi}, W \cdot m^{-1} \cdot K^{-1}$	TS2C	TS2C_NF	TS2C	TS2C_NF
120	0.611	0.721	0.502	0.531
130	0.614	0.725	0.503	0.5325
145	0.617	0.730	0.5045	0.534

Fig. 4 Ternary picture generated using thresholds of 55 and 142 (Durabrade 1605 powder)

Table 3 Predicted effective thermal conductivities based on the ternary picture

	$\kappa_e, W \cdot m^{-1} \cdot K^{-1}$ (Durabrade powder/ternary picture)
TS2C	0.551
TS2C_NF	0.669

perform that step, a small C program was written because it is not so easy to generate ternary pictures on the basis of standard image manipulation software packages such as imageJ.

Figure 4 presents the ternary picture generated from these darker regions observed on the initial microstructure (Fig. 3a). The thresholds used to generate this picture were 55 and 142 for the pore/polyester and polyester/AlSi transitions, respectively. This ternary picture presents a porosity level of 4.2%, a polyester content of 62.6% and an AlSi content of 33.2% (i.e., similar to Fig. 3b). Table 3 summarizes the computed effective thermal conductivities based on Fig. 4 assuming thermal conductivities of $130 \ W \cdot m^{-1} \cdot K^{-1}$ for the AlSi phase

(white), $0.17 \ W \cdot m^{-1} \cdot K^{-1}$ for the polyester (gray) and $0.025 \ W \cdot m^{-1} \cdot K^{-1}$ for the pores (i.e., black pixels). The values were calculated using the cell-centered and nodal formulations of TS2C.

The values of 0.551 and $0.669 \ W \cdot m^{-1} \cdot K^{-1}$ can be compared to the values of 0.614 and 0.725 contained in Table 2, respectively: the difference results from the additional pore phase suggested in Fig. 4.

4.3 Coatings Produced with the Metco Powder

Figure 5 presents the coatings produced with the Metco 601 NS powder. The initial microstructure is shown in
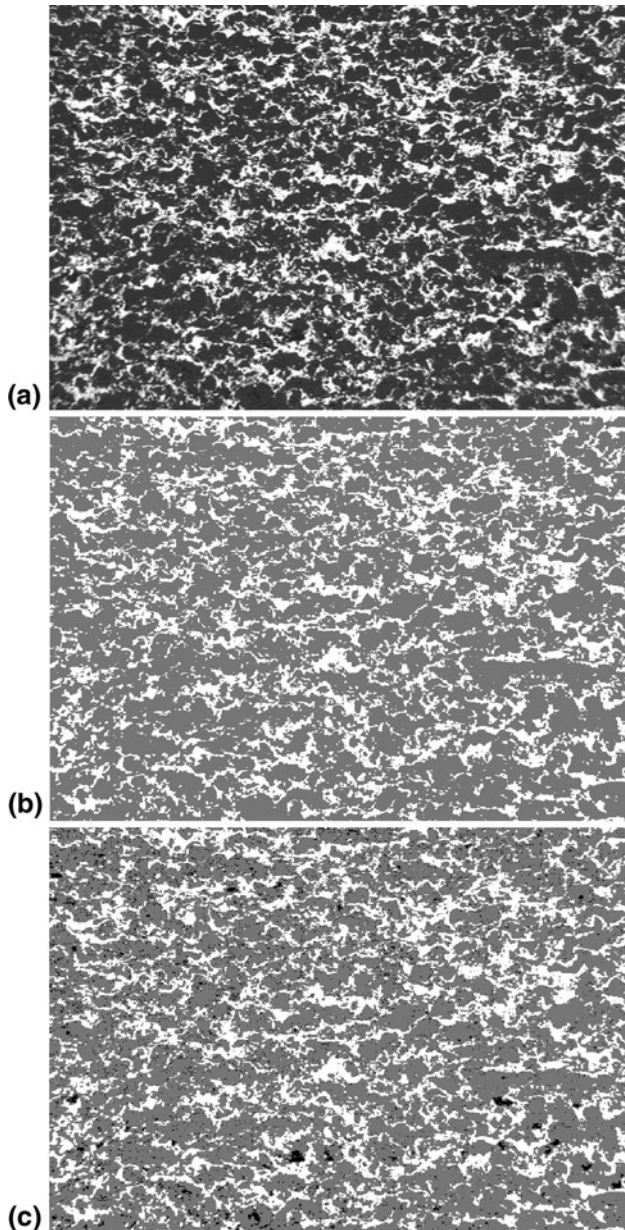

Fig. 5 Pictures concerning the coating produced with Metco 601 NS powder—microstructure (a), binary picture (b), and ternary picture (c)

Fig. 5(a), the binary picture obtained using a threshold of 142 is presented on Fig. 5(b), and the ternary picture produced using thresholds of 55 and 142 is shown on Fig. 5(c). The ternary picture presents a porosity level of 2.8%, a polyester rate of 69.6%, and an AlSi content of 27.6%. For the binary picture, the pore and polyester rates are cumulated. In comparison with the case of the Durabrade 1605 powder, the AlSi content is 5.6% lower (27.6% against 33.2%) which represent a significant difference.

Table 4 summarizes the results obtained for the coating produced with the Metco 601 NS powder. Since the AlSi content is lower in comparison with the coatings produced with the Durabrade powder, the predicted effective thermal conductivities are lower, but tendencies remain similar: the computed values obtained with the nodal formulation of TS2C are higher than those computed for the cell-centered formulation and the use of a ternary picture in which the pores are differentiated from the polyester phase provides a lower thermal conductivity. Concerning the experimental measurements, the measured value was the same for the coatings produced with both powders (i.e., $0.53 \ W \cdot m^{-1} \cdot K^{-1}$).

4.4 Splitting the Pixels into Multiple Cells

Since the results obtained for the cell-centered and nodal formulations present differences which tend to decrease with the picture resolution, our last efforts were devoted to the development of a new method including four cells (or more) in each pixel. With that method, the calculated thermal conductivities tend to converge to a single value.

Table 5 presents an overview of the results obtained for the different cases considered versus picture resolution. Since these results were found to be weakly sensitive regarding to the value assumed for the thermal conductivity of AlSi, only the results calculated for the value of $130 \ W \cdot m^{-1} \cdot K^{-1}$ are reported in the table.

The powder type is given in column 1. The image type is given in column 2 in which *Despec* means that the image was treated using successive Despeckle filtering, *Binary* means that the picture contains two phases only (AlSI + polyester), whereas *Ternary* corresponds to the pictures in which the pores were differentiated from the polyester phase. The software package (or version) is given in column 3 in which CC means cell-centered and NF means nodal formulation of TS2C. The last column (case 200%)

Table 4 Summary of the results obtained for the micrograph corresponding to the coating produced with the Metco 601 NS powder (Fig. 6)

κ_e, W· m^{-1}· K^{-1} (Metco 601 NS powder)			
Binary picture		Ternary picture (i.e., pore/ polyester differentiation)	
TS2C	TS2C_NF	TS2C	TS2C_NF
0.486	0.562	0.455	0.537

concerns the calculations in which each pixel was split into four cells. Table 5 indicates that the asymptotic value obtained for the initial image treated using successive Despeckle filtering (42, 44) (see Table 1) is about $0.48 \ \text{W} \cdot \text{m}^{-1} \cdot \text{K}^{-1}$. For nonsimplified images, the difference between the results produced with the nodal and cell-centered formulations remains higher (i.e., about 10% of the absolute value of the thermal conductivity when each pixel is split into four cells).

Figure 6 plots the results of Table 5. The first curve (horizontal line) corresponds to the measured value. Curves 2 to 4 concern the picture obtained for the Durabrade powder after treatment using Despeckle filtering (i.e., data of Table 1 completed by the results obtained for the nodal formulation of TS2C). One may see that the curves obtained for the nodal version of TS2C and with OOF2 are very close one from the other, the common point being that both use a nodal discretization method. Curves 5 to 8 concern the Durabrade powder, whereas curves 9 to 12 concern the results obtained for the Metco

powder. Curves 5 and 6 (dashed double dot line with hollow circles) concern the binary picture obtained for the Durabrade powder and treated using either the cell-centered or nodal formulations of TS2C. Curves 7 and 8 (dashed line with hollow squares) concern the same data but for the ternary picture. Curves 9 and 10 (short dashed line with hollow lozenges) concerns the same as 5 and 6, but for the Metco powder instead of the Durabrade powder. Finally, curves 11 and 12 (dash dotted line with hollow triangles) concern the same as 7 and 8 but for the Metco powder (i.e., ternary picture treated with the nodal or cell-centered formulations). In each case, the curves obtained with a cell-centered formulation present an increasing tendency versus the increase of the picture resolution. On the contrary, the curves obtained using a nodal formulation (OOF2 + TS2C_NF), present always a decreasing tendency. In each case, the results obtained using either a nodal or cell-centered formulation, are converging when increasing the picture resolution, which means that all attempts to simplify the architecture may affect the calculated results.

5. Conclusions

This study was devoted to the estimation of the homogenized thermal conductivity of AlSi/polyester abradable coatings. It was supported by the European Commission through the NEWAC European project leaded by MTU Aero Engines. New developments were performed in the in-house TS2C code to satisfy the needs of the project. The differences previously noticed concerning the results predicted with OOF2 and TS2C may be explained by the discretization method (nodal formulation in OOF2 and cell-centered formulation in the initial version of TS2C). The numerical computations are in accuracy with the measured values. However, it is difficult to
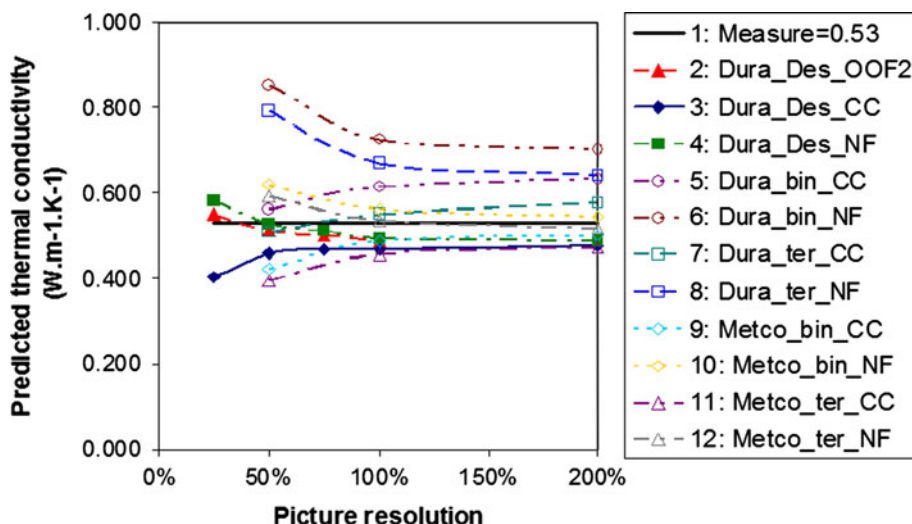
Table 5 Summary of the thermal conductivities calculated for the different cases

Powder used	Image type	OOF/TS2C	Picture resolution		
			50%	100%	200%
Durabrade 1605	Despec Fig. 1 (Ref 3, 4)	OOF2	0.511	0.485	NA
		CC	0.458	0.467	0.474
		NF	0.528	0.493	0.485
	Binary Fig. 4 mid	CC	0.561	0.614	0.634
		NF	0.852	0.725	0.701
	Ternary Fig. 5	CC	0.507	0.551	0.574
		NF	0.791	0.669	0.641
Metco 601 NS	Binary Fig. 6 mid	CC	0.421	0.486	0.500
		NF	0.619	0.562	0.545
	Ternary Fig. 6 bot	CC	0.395	0.455	0.471
		NF	0.593	0.537	0.518

Fig. 6 Summary of the results computed for the different pictures (raw or after Despeckle filtering, Durabrade or Metco, binary or ternary) and treated using either the cell-centered or nodal formulations of TS2C (+OOF2 for pictures treated using Despeckle)

conclude concerning the superiority of one of the two formulations versus the other. Our final recommendations are the following ones: first, the micrographs used to estimate the effective thermal conductivities should cover a sufficiently large area (minimum extend of 2 mm in the horizontal direction) for the present application. This minimal area is linked to the representative volume of the material below which the calculations are diverging (mainly because of an increase of the connectivity of AlSi). Second, there is no justification in applying simplifications of the structure (such as Despeckle filtering). Hence, the binary or ternary pictures directly based on the raw micrographs can serve as input data for the thermal conductivity evaluation. Third, the calculated thermal conductivities are not sensitive versus the thermal conductivity of the conductive phase (i.e., AlSi in the present case). Fourth, in future works, special efforts will have to be paid to the differentiation of the pores relatively to the polyester phase because it was shown that the results are sensitive to the pore content even for a pore level of 4%.

Acknowledgment

References

1. G. Antou, F. Hlawka, A. Cornet, C. Becker, D. Ruch, and A. Riche, In Situ Laser Remelted Thermal Barrier Coatings: Thermophysical Properties, *Surf. Coat. Technol.*, 2006, **200**, p 6062

2. W.J. Parker, R.J. Jenkins, C.P. Butler, and G.L. Abbott, Flash Method of Determining Thermal Diffusivity, Heat Capacity, and Thermal Conductivity, *J. Appl. Phys.*, 1961, **32**(9), p 1679-1684

3. H. Wang and R.B. Dinwiddie, Reliability of Laser Flash Thermal Diffusivity Measurements of the Thermal Barrier Coatings, *J. Thermal Spray Technol.*, 2000, **9**(2), p 210-214

4. P.G. Klemens, Thermal Conductivity of Inhomogeneous Media, *High Temp High Press.*, 1991, **23**(3), p 241-248

5. K.W. Schlichting, N.P. Padture, and P.G. Klemens, Thermal Conductivity of Dense and Porous Yttria-Stabilized Zirconia, *J. Mater. Sci.*, 2001, **36**, p 3003-3010

6. J. Wu, N.P. Padture, P.G. Klemens, M. Gell, E. Garcia, P. Miranzo, and M.I. Osendi, Thermal Conductivity of Ceramics in the ZrO2-GdO1.5 System, *J. Mater. Res.*, 2002, **17**(12), p 3193-3200

7. J. Wu, X. Wei, N.P. Padture, P.G. Klemens, M. Gell, E. Garcia, P. Miranzo, and M.I. Osendi, Low-Thermal-Conductivity Rare-Earth Zirconates for Potential Thermal-Barrier-Coating Applications, *J. Am. Ceram. Soc.*, 2002, **85**(12), p 3031-3035

8. L. Braginsky, V. Shklover, G. Witz, and H.-P. Bossmann, Thermal Conductivity of Porous Structures, *Phys. Rev. B*, 2007, **75**, p 094301

9. S. Raghavan, H. Wang, R.B. Dinwiddie, W.D. Porter, and M.J. Mayo, The Effect of Grain Size, Porosity and Yttria Content on the Thermal Conductivity of Nanocrystalline Zirconia, *Scripta Mater.*, 1998, **39**(8), p 1119-1125

10. D.P.H. Hasselman, Effect of Cracks on Thermal Conductivity, *J. Comp. Mater.*, 1978, **12**(10), p 403-407

11. R. Dutton, R. Wheeler, K.S. Ravichandran, and K. An, Effect of Heat Treatment on the Thermal Conductivity of Plasma-Sprayed Thermal Barrier Coatings, *J. Thermal Spray Technol.*, 2000, **9**(2), p 204-209

12. F. Cernuschi, P. Bianchi, M. Leoni, and P. Scardi, Thermal Diffusivity/Microstructure Relationship in Y-PSZ Thermal Barrier Coatings, *J. Thermal Spray Technol.*, 1999, **8**(1), p 102-109

13. R. McPherson, A Model for the Thermal Conductivity of Plasma-Sprayed Ceramic Coatings, *Thin Solid Films*, 1984, **112**, p 89-95

14. S. Boire-Lavigne, C. Moreau, and R.G. Saint-Jacques, The Relationship Between the Microstructure and Thermal Diffusivity of Plasma-Sprayed Tungsten Coatings, *J. Thermal Spray Technol.*, 1995, **4**(3), p 261-267

15. I. Sevostianov and M. Kachanov, Anisotropic Conductivities of Plasma Sprayed Thermal Barrier Coatings in Relation to the Microstructure, *J. Thermal Spray Technol.*, 2000, **9**(4), p 478-482

16. I. Sevostianov and M. Kachanov, Plasma-Sprayed Ceramic Coatings: Anisotropic Elastic and Conductive Properties in Relation to the Microstructure; Cross-Property Correlations, *Mater. Sci. Eng. A*, 2001, **297**, p 235-243

17. I. Sevostianov and M. Kachanov, On the Yield Condition for Anisotropic Porous Materials, *Mater. Sci. Eng. A*, 2001, **313**, p 1-15

18. I. Sevostianov, L. Gorbatikh, and M. Kachanov, Recovery of Information on the Microstructure of Porous/Microcracked Materials from the Effective Elastic/Conductive Properties, *Mater. Sci. Eng. A*, 2001, **318**, p 1-14

19. I. Sevostianov, M. Kachanov, J. Ruud, P. Lorraine, and M. Dubois, Quantitative Characterization of Microstructures of Plasma-Sprayed Coatings and Their Conductive and Elastic Properties, *Mater. Sci. Eng. A*, 2004, **386**, p 164-174

20. I. Sevostianov and M. Kachanov, Elastic and Conductive Properties of Plasma-Sprayed Ceramic Coatings in Relation to Their Microstructure—An Overview, *J. Thermal Spray Technol.*, 2009, **18**(5-6), p 822-834

21. I.O. Golosnoy, S.A. Tsipas, and T.W. Clyne, An Analytical Model for Simulation of Heat Flow in Plasma-Sprayed Thermal Barrier Coatings, *J. Thermal Spray Technol.*, 2005, **14**(2), p 205-214

22. I.O. Golosnoy, A. Cipitria, and T.W. Clyne, Heat Transfer Through Plasma-Sprayed Thermal Barrier Coatings in Gas Turbines: A Review of Recent Work, *J. Thermal Spray Technol.*, 2009, **18**(5-6), p 809-821

23. E.Y. Litovsky and M. Shapiro, Gas Pressure and Temperature Dependences of Thermal Conductivity of Porous Ceramic Materials: Part 1, Refractories and Ceramics with Porosity below 30%, *J. Am. Ceram. Soc.*, 1992, **75**(12), p 3425-3439

24. E. Litovsky, T. Gambaryan-Roisman, M. Shapiro, and A. Shavit, Heat Transfer Mechanisms Governing Thermal Conductivity of Porous Ceramic Materials, *Trends Heat Mass Momentum Transf.*, 1997, **3**, p 147-167

25. E. Litovsky, T. Gambaryan-Roisman, M. Shapiro, and A. Shavit, Novel Heat-Transfer Mechanisms Affecting the Thermal Conductivity of Porous Ceramics, *High Temp. High Press.*, 2001, **33**, p 27-33

26. E. Litovsky, S. Horodetsky, and J. Kleiman, Non-Destructive Thermal Diagnostics of Porous Materials, *Int. J. Thermophys.*, 2005, **26**(6), p 1815-1831

27. K.J. Hollis, Pore Phase Mapping and Finite-Element Modeling of Plasma Sprayed Tungsten Coatings, *Thermal Spray Science & Technology*, C.C. Berndt and S. Sampath, Ed., ASM Int, Materials Park, OH, 1995, p 403-408

28. K. Bakker, Using the Finite Element Method to Compute the Influence of Complex Porosity and Inclusion Structures on the Thermal and Electrical Conductivity, *Int. J. Heat Mass Transf.*, 1997, **40**(15), p 3503-3511

29. A. Kulkarni, Z. Wang, T. Nakamura, S. Sampath, A. Goland, H. Herman, J. Allen, J. Ilavsky, G. Long, J. Frahm, and R.W. Steinbrech, Comprehensive Microstructural Characterization and Predictive Property Modeling of Plasma-Sprayed Zirconia Coatings, *Acta Mater.*, 2003, **51**, p 2457-2475

30. Z. Wang, A. Kulkarni, S. Deshpande, T. Nakamura, and H. Herman, Effects of Pores and Interfaces on Effective Properties of Plasma Sprayed Zirconia Coatings, *Acta Mater.*, 2003, **51**, p 5319-5334

31. Y. Tan, J.P. Longtin, and S. Sampath, Modeling Thermal Conductivity of Thermal Spray Coatings: Comparing Predictions to Experiments, *Proceedings of the International Thermal Spray Conference*, Seattle, 2006
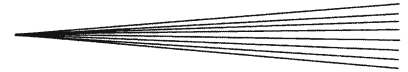
32. P. Michlik and C.C. Berndt, Image-Based Extended Finite Element Modeling of Thermal Barrier Coatings, *Surf. Coat. Technol.*, 2006, **201**, p 2369-2380

33. A.D. Jadhav, N.P. Padture, E.H. Jordan, M. Gell, P. Miranzo, and E.R. Fuller, Jr., Low-Thermal-Conductivity Plasma-Sprayed Thermal Barrier Coatings with Engineered Microstructures, *Acta Mater.*, 2006, **54**, p 3343-3349

34. J.M. Dorvaux, O. Lavigne, R. Mévrel, M. Poulain, Y. Renollet, and C. Rio, Modelling the Thermal Conductivity of Thermal Barrier Coatings, *Proc. 85th AGARD SMP Meeting on Thermal Barrier Coatings*, 1997

35. R. Bolot, G. Antou, G. Montavon, and C. Coddet, A two-Dimensional Heat Transfer Model for Thermal Barrier Coating Average Thermal Conductivity Computation, *Numer. Heat Transf. A*, 2005, **47**(9), p 875-898

36. R. Bolot, G. Antou, G. Montavon, and C. Coddet, Calcul Numérique de la Conductivité Thermique de Dépôts de Zzircone Yttriée Elaborés par Projection Thermique, *Proceedings of MATERIAUX 2006*, November 13-17 (Dijon, France), 2006 (in French)

37. G. Antou, G. Montavon, F. Hlawka, A. Cornet, C. Coddet, and F. Machi, Modification of Thermal Barrier Coating Architecture by In Situ Laser Remelting, *J. Eur. Ceram. Soc.*, 2006, **26**, p 3583-3597

38. S. Costil, C. Verdy, R. Bolot, and C. Coddet, On the Role of Spraying Process on Microstructural, Mechanical, and Thermal Response of Alumina Coatings, *J. Thermal Spray Technol.*, 2007, **16**(5-6), p 839

39. R. Bolot, J.H Qiao, P. Bertrand, G. Bertrand, and C. Coddet, Effect of Thermal Treatment on the Effective Thermal Conductivity of YPSZ coatings, *Surf. Coat. Technol.*, 2010, in press

40. http://www.newac.org

41. http://www.newac.org/uploads/media/No.06_UTBM_Euromat.pdf)

42. R. Bolot, J.L. Seichepine, F. Vucko, C. Coddet, D. Sporer, P. Fiala, and B. Bartlett, Thermal Conductivity of AlSi/Polyester Abradable Coatings, *Thermal Spray Crossing Borders*, E. Lugscheider, Ed., June 2-4, 2008 (Maastricht, The Netherlands), DVS, DE, 2008

43. R. Bolot, J.L. Seichepine, F. Vucko, C. Coddet, D. Sporer, P. Fiala, and B. Bartlett, Thermal Conductivity of AlSi/Polyester Abradable Coatings, *Weld Cut*, 2009, **8**(2), p 104-109

44. http://www.matweb.com

45. http://techtran.msfc.nasa.gov/tech_ops/nasa388alloy.pdf

46. http://www.substech.com

Peer Reviewed